


# Automated detection of hyperreflective foci in the outer nuclear layer of the retina

Mathias Falck Schmidt<sup>1</sup>  | Jakob Lønborg Christensen<sup>2</sup> | Vedrana Andersen Dahl<sup>2</sup> | Ahmed Toosy<sup>3</sup> | Axel Petzold<sup>4,5,6</sup> | James V. M. Hanson<sup>7</sup> | Sven Schippling<sup>8</sup> | Jette Laurup Frederiksen<sup>9</sup> | Michael Larsen<sup>10</sup>

<sup>1</sup>Department of Neurology, Clinic of Optic Neuritis, The Danish Multiple Sclerosis Center (DMSC), Rigshospitalet, Glostrup, Denmark

<sup>2</sup>Department of Applied Mathematics and Computer Science, Technical University of Denmark, Lyngby, Denmark

<sup>3</sup>NMR Research Unit, Queen Square Multiple Sclerosis Centre, Department of Neuroinflammation, Queen Square UCL Institute of Neurology, University College London, London, UK

<sup>4</sup>Moorfields Eye Hospital NHS Foundation Trust, London, UK

<sup>5</sup>Neuro-ophthalmology Expertise Centre, University Medical Centre, University of Amsterdam, Amsterdam, The Netherlands

<sup>6</sup>UCL Institute of Neurology, London, UK

<sup>7</sup>Department of Ophthalmology, University Hospital Zurich and University of Zurich, Zurich, Switzerland

<sup>8</sup>Multimodal Imaging in Neuroimmunological Diseases (MINDS), University Hospital Zurich and University of Zurich, Zurich, Switzerland

<sup>9</sup>Department of Neurology, Clinic of Optic Neuritis, The Danish Multiple Sclerosis Center (DMSC), Rigshospitalet and University of Copenhagen, Glostrup, Denmark

<sup>10</sup>Department of Ophthalmology, Rigshospitalet and University of Copenhagen, Glostrup, Denmark

## Correspondence

Mathias Falck Schmidt, MD, Department of Neurology, Clinic of Optic Neuritis, The Danish Multiple Sclerosis Center (DMSC), Rigshospitalet, Valdemar Hansens Vej 13, 2600 Glostrup, Denmark.  
Email: [mathias.falck.schmidt@regionh.dk](mailto:mathias.falck.schmidt@regionh.dk)

## Abstract

**Purpose:** Hyperreflective foci are poorly understood transient elements seen on optical coherence tomography (OCT) of the retina in both healthy and diseased eyes. Systematic studies may benefit from the development of automated tools that can map and track such foci. The outer nuclear layer (ONL) of the retina is an attractive layer in which to study hyperreflective foci as it has no fixed hyperreflective elements in healthy eyes. In this study, we intended to evaluate whether automated image analysis can identify, quantify and visualize hyperreflective foci in the ONL of the retina.

**Methods:** This longitudinal exploratory study investigated 14 eyes of seven patients including six patients with optic neuropathy and one with mild non-proliferative diabetic retinopathy. In total, 2596 OCT B-scan were obtained. An image analysis blob detector algorithm was used to detect candidate foci, and a convolutional neural network (CNN) trained on a manually labelled subset of data was then used to select those candidate foci in the ONL that fitted the characteristics of the reference foci best.

**Results:** In the manually labelled data set, the blob detector found 2548 candidate foci, correctly detecting 350 (89%) out of 391 manually labelled reference foci. The accuracy of CNN classifier was assessed by manually splitting the 2548 candidate foci into a training and validation set. On the validation set, the classifier obtained an accuracy of 96.3%, a sensitivity of 88.4% and a specificity of 97.5% (AUC 0.989).

**Conclusion:** This study demonstrated that automated image analysis and machine learning methods can be used to successfully identify, quantify and visualize hyperreflective foci in the ONL of the retina on OCT scans.

## KEY WORDS

convolutional neural network, hyperreflective foci, outer nuclear layer of the retina, optical coherence tomography

Jette Laurup Frederiksen and Michael Larsen are shared last authorship.

This is an open access article under the terms of the [Creative Commons Attribution](https://creativecommons.org/licenses/by/4.0/) License, which permits use, distribution and reproduction in any medium, provided the original work is properly cited.

© 2022 The Authors. *Acta Ophthalmologica* published by John Wiley & Sons Ltd on behalf of Acta Ophthalmologica Scandinavica Foundation.

## 1 | INTRODUCTION

Originally, the term ‘hyperreflective foci’ was used to define any hyperreflective lesion, dotted or focal in appearance, when imaged using optical coherence tomography (OCT) at any retinal layer (Fragiotta et al., 2021). The presence of hyperreflective foci was first described in diabetic macular oedema as a morphologic sign of lipid extravasation (Bolz et al., 2009). However, in the past decade, hyperreflective foci have been characterized in a considerable amount of different retinal disorders and with the use of various of morphological entities such as migrating retinal pigment epithelium cells, macrophages/microglia in age-related macular degeneration (AMD) (Curcio et al., 2017; Framme et al., 2010; Pang et al., 2015) and degenerated photoreceptor cells (Torm et al., 2020; Uji et al., 2012). Furthermore, a cell-sized migrating intraretinal hyperreflective element has been observed incidentally in a healthy child (Torm et al., 2020).

Although no consensus about the origin of hyperreflective foci exists (Wang et al., 2011), studies suggest that hyperreflective foci may represent aggregates of activated microglia (S. Vujosevic et al. 2013). In contrast, retinal exudates, microaneurysms and haemorrhages are all classified as subtypes of ‘hyperreflective elements’ and can be distinguished from the hyperreflective foci phenotype based on specific morphological characteristics (Kodjikian et al., 2019).

Hyperreflective foci are not detectable by fundus photography and their occasional presence in healthy subjects suggests that they are distinct from hard exudates. They are currently being investigated as a clinically accessible in vivo diagnostic and prognostic biomarker of potential interest in a broad spectrum of retinal disorders (Abri Aghdam et al., 2015; Altay et al., 2016; Borrelli et al., 2019; Busch K. et al., 2020; Chen et al., 2016; Fragiotta et al., 2018). The manual mapping and counting of hyperreflective foci are a time-consuming process. Therefore, the development and application of tools to effectively visualize and quantify the presence and flux of hyperreflective foci is of great importance and may assist in the clinical diagnosis and in the monitoring of progression and treatment response.

In this study, we determined whether an image analysis pipeline consisting of a convolutional neural network (CNN) classifier may be used for accurate quantification and visualization of hyperreflective foci in the outer nuclear layer of the retina. The avascular outer nuclear layer of the retina was of particular interest in this study because hyperreflective foci imaged on OCT within this region could be assumed to represent true foci, not vessels.

## 2 | MATERIALS AND METHODS

In this exploratory longitudinal study, we investigated six patients presenting with an ophthalmoscopically normal fundus and one patient with reversible fundus abnormalities (see patient characteristics, Table 1). An ethical waiver for the use of anonymized data from each patient was obtained. The study was conducted in agreement

with the Tenets of the Declaration of Helsinki and was approved by the local Ethics Committee. Fourteen eyes of seven patients were evaluated.

In every patient, two to four OCT examinations were performed for each eye, over time (see supplemental material). We acquired in total, 2596 B-scans across all time points and patients. All B-scans were examined by one independent examiner who was blinded to the clinical characteristics of the patients (e.g. age, gender, visual function and diagnosis). The examiner manually labelled hyperreflective foci in the outer nuclear layer, defined as the region between the outer plexiform layer and retinal pigment epithelium (RPE) line. Hyperreflective foci were manually annotated according to the following fundamental features: (i) location within the outer retina; (ii) size  $\leq 30\mu\text{m}$ ; (iii) absence of a shadow cast by the hyperreflective foci and (iv) reflectivity similar to the retinal nerve fibre layer (RNFL). In the latest international consensus guidelines, these morphological characteristics were incorporated as the diagnostic criteria for hyperreflective foci (Kodjikian et al., 2019; Lee & Chung, 2018; Midena et al., 2018). In total, 391 hyperreflective foci were manually annotated among the 189 B scans originating from nine eyes of seven patients.

### 2.1 | Automatic detection of hyperreflective foci

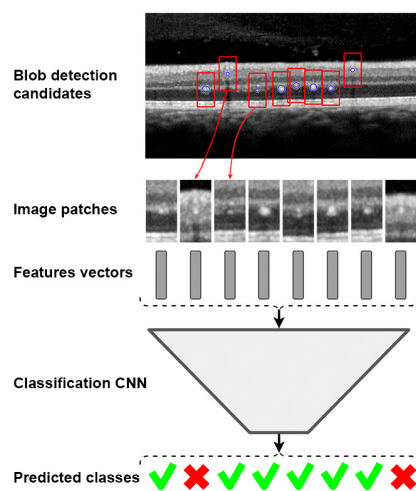
The hyperreflective foci detection method comprises (1) candidate detection, (2) feature extraction and (3) candidate classification (see Figure 1). Candidate detection uses ‘blob’ detection (Lindeberg, 1996) and detects likely candidates for hyperreflective foci (blobs) in the image. Feature extraction extracts a set of measurements for each of the candidates detected in the first step. The features are radius and the intensity of the detected hyperreflective foci candidate, proximity to a blood vessel in the retina, and the location within the retinal layer where the hyperreflective focus candidate was detected. We applied layer detection (Li et al., 2016; Haeker et al., 2007) to find the retinal layers. Furthermore, image patches centred around hyperreflective foci candidates were extracted. The third part, feature classification, uses CNN for classification of the extracted patches and the features.

The 2548 B-scans for the classification consisted of positive and negative hyperreflective foci candidates found by blob detection. As we report in the results section, there was a large-class imbalance in this data set with 350 positive and 2198 negative candidates. To alleviate the class imbalance, we oversampled the positive examples.

Data were divided into training (80%) and validation (20%) sets. The CNN was trained on the training data. However, the CNN performance on the on-validation data was slightly biased as we did not split specific images or eyes into a test and training set. When we assessed the classification on the validation set, the CNN may have seen a training example originating from the same patient, eye (volume) or even specific B-scan giving rise to unwanted bias.

**TABLE 1** Demographical and clinical characteristics of the individual patients are presented (i.e. diagnosis, best corrected visual acuity in Snellen decimal notation, visual field tests and treatment)

Patient characteristics			
Gender			
Male/female ratio	2/5		
Age-years			
Median (range)	37 (20–39)		
Diagnosis	Best corrected visual acuity	Visual field	Treatment
Patient No. 1 Diagnosis 'left optic nerve lesion unknown cause'	At initial presentation: Right eye: 1.0 Left eye: 0.2 After 7 months Right eye: 1.0 Left eye: 0.5	Visual field defects on left eye	Treated with Solu-medrol 1000mg intravenous (IV) for 3 days
Patient No.2 Type 1 diabetes mild, non-proliferative retinopathy. Diagnosis of left optic atrophy	At initial presentation: Right eye: 1.0 Left eye: not recordable. 1 month later: Right eye: 1.0 Left eye: 0.1	Left-sided hemianopia with macula sparing on right eye Left eye not recordable	IV Solu-medrol
Patient No.3 Presumed left NA-AION	At initial presentation: Right eye: not recordable Left eye: 0.8	Visual field defect on left eye (mostly infero-temporal)	Solu-Medrol IV, Nexium
Patient No.4 Left optic neuritis	At initial presentation: Right eye: 1.0 Left eye: 0.25	Left centrocecal scotoma	No medication given.
Patient No.5 Diagnosis 'optic neuritis' of unknown cause	n/a.		
Patient No.6 Diagnosis of right optic neuritis, most likely an isolated episode of neuroretinitis	At initial presentation: Right eye: 1.0 Left eye 1.0	Loss of vision in the right eye Visual field was full to red pin in left eye	No medication given.
Patient No.7 Left acute optic neuropathy	At initial presentation: Right eye: 1.0 Left eye 0.1 6 months later Right eye: 1.0 Left eye: 0.6	The right eye was normal. Peripheral field loss in the left eye.	Amitriptyline 50mg Azathioprine 50mg twice daily

**FIGURE 1** Visualization of the method pipeline showing candidate foci in the outer nuclear layer that were sufficiently separated from the hyperreflective outer plexiform layer (✓) and candidate foci that are embedded within the ganglion cell layer/inner plexiform layer (✗).

## 2.2 | OCT acquisition

The development of robust AI algorithms using supervised learning benefits from large and heterogeneous training data sets. Hence, different retinal disorders were examined in this study and data were acquired from different OCT scanning protocols. All patients underwent OCT imaging with Spectralis OCT machines (Heidelberg Engineering, Heidelberg, Germany, software version 6.0.13). Five of the scan protocols comprised a peripapillary ring scan (circular scans with 15 degrees diameter, Automatic Real-Time [ART] 15–25) and a macular volume scan (scan centred on the fovea with 30×15 degrees, 19 vertical B-scans, ART, B-scan distance varies from 239–256 μm). In the last two scan protocols, OCT data originate from peripapillary ring scans (circular scans with 15 degrees' diameter, ART set from 15 to 25) and macular volume scans (scans centred on the fovea with 20×20 degrees, 25 vertical B-scans, ART 15–50, B-scan distance varied from 234–250 μm). All scans were performed in high-resolution mode with eye

**TABLE 2** Confusion matrix used for evaluating the performance of the blob classification model on validation data

CNN classifier	Ground truth = 1	Ground truth = 0
Prediction = 1	61 (88.4%)	11 (2.5%)
Prediction = 0	8 (11.6%)	430 (97.5%)

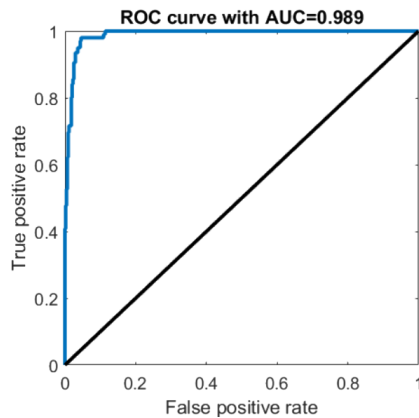


**FIGURE 2** Receiver operator curve (ROC) the validation data set. The area under the curve (AUC) is 0.989.

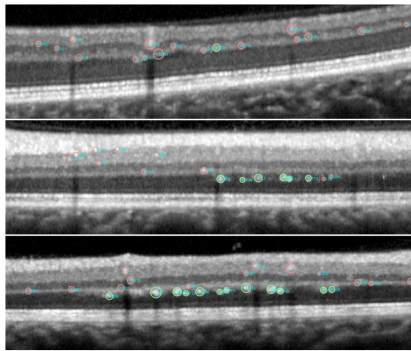


**FIGURE 3** Examples of the classification method. In patient 1, the CNN classifier detects foci pattern (green circles) from the non-foci pattern (red circles) in the outer nuclear layer of the retina.

tracking enabled. The OSCAR-IB criteria were used to assess the quality of the retinal OCT scans, and we report results in agreement with the Advised Protocol for OCT Study Terminology and Elements (APOSTEL).

### 3 | RESULTS

In the manually labelled data set, the blob detector found in total 2548 candidate foci. The algorithm correctly detected 350 out of the 391 manually annotated hyperreflective foci, indicating that the blob detector misses around 11% of hyperreflective foci, identified as true foci by the grader.

The CNN classifier confusion matrix can be seen in Table 2. The accuracy of CNN classifier was assessed by splitting the 2548 detections in the manually labelled data set into training (80%) and validation (20%) data sets. On the validation data set, the classifier

obtained an accuracy of 96.3%, a sensitivity of 88.4% and a specificity of 97.5%. Corresponding receiver operating characteristic (ROC) curve on the validation set achieved an area under the curve of 0.989 (see ROC curve, Figure 2). Examples of the classification method and heatmap visualizations of hyperreflective foci are shown in Figures 3–5. A box plot showing the distribution of data obtained from feature extraction can be seen in Figure 6.

### 4 | DISCUSSION

This longitudinal exploratory study demonstrated that our automated image analysis pipeline performed successfully with an overall high accuracy of the CNN classification (AUC of 0.989) at detecting hyperreflective foci in the outer nuclear layer.

In general, image segmentation is a problem often tackled with deep learning architectures such as a UNet (Ronneberger et al., 2015). However, a UNet would not be able to reliably segment the hyperreflective foci for multiple reasons in this study. Our data comprise OCT images that often possessed only a small number of hyperreflective foci. Consequently, there would not be enough data to train a UNet since a single data point for a UNet is a full image. A large data set with thousands or at least hundreds of data points is necessary when training deep learning-based algorithms. If a data point is a single hyperreflective focus instead, then the lack of data is much less problematic. In this case, we have 391 positive data points along with thousands of negative data points. The segmentation pipeline therefore consists of first locating likely hyperreflective foci with blob analysis and then classifying them with a CNN. A segmentation problem is essentially converted into a classification one. The features we extracted are useful in helping the CNN classify hyperreflective foci. Additionally, they provide useful information about, for example the distribution of foci radii and the retinal layer position of the hyperreflective foci. These features could potentially inform which characteristics of hyperreflective foci are associated with healthy/unhealthy specimens. A naive UNet segmentation would be unable to extract these features.

The frequent presence of hyperreflective foci with OCT calls for a systematic study of their appearance, location, density, movement, disappearance and associated health characteristics. In this study, we only considered ophthalmoscopically normal eyes or eyes with reversible abnormalities on fundusoscopic examination. The approach in many prior studies has been to look at severely abnormal conditions such as radiation retinopathy (Frizziero et al., 2016) or neovascular AMD (Mokhtari et al., 2017). In this study, we investigated conditions with no confounding elements of structural abnormalities in the retina which improved the algorithm robustness. This approach is potentially applicable in conditions with scant hyperreflective foci such as multiple sclerosis (Pilotto et al., 2020), where the retina may be relatively normal, and therefore it is easier to train automated image analysis systems.



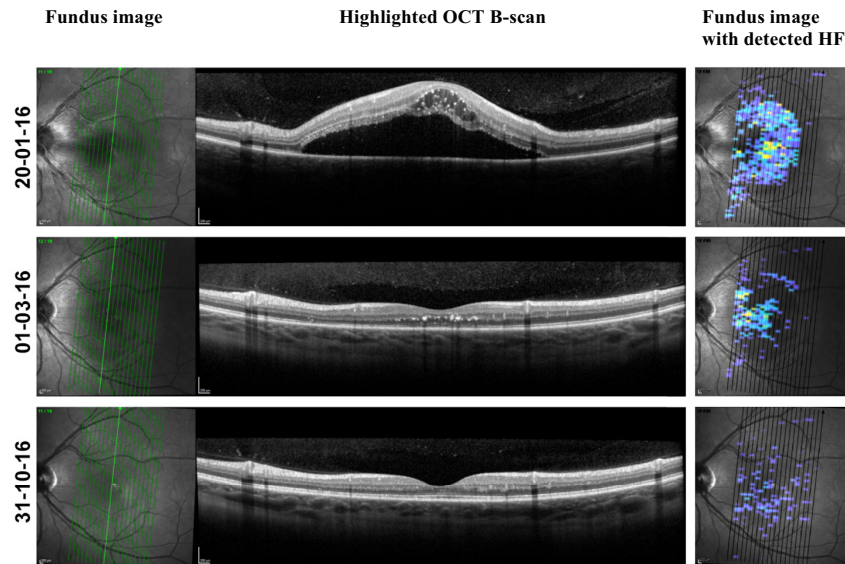


**FIGURE 4** OCT B-scans presented at three different dates on same location in the left retina of patient 2. The highlighted slice at the left fundus image is shown in the middle. A heatmap of detected hyperreflective foci is overlaid on the fundus image (right). HF, hyperreflective foci.

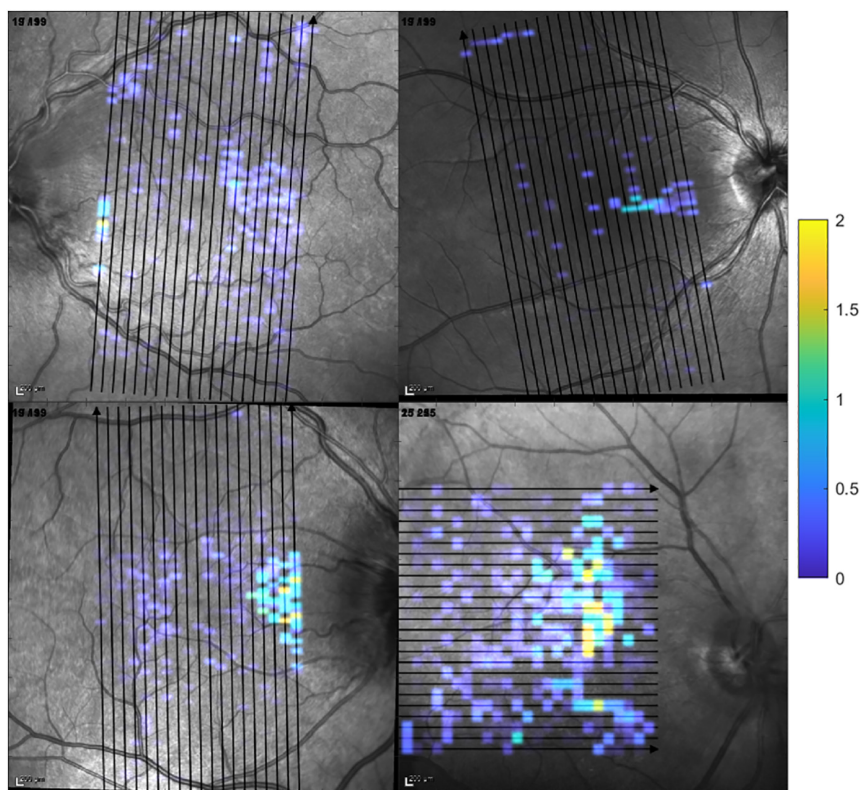


**FIGURE 5** Fundus images with overlaid heatmap of detected hyperreflective foci in patient 3, 4, 6 and 7.

Currently, very few studies concerning the automated or semi-automated detection of retinal hyperreflective foci have been performed (Varga et al., 2019; Yu et al., 2019). These studies are criticized for being unreliable and applicable only from an informative and technical point of view (Midená et al., 2021). Moreover, these studies often examine both the inner and outer retinal layers where it can be challenging to distinguish between vessels and intraretinal hyperreflective elements. To overcome this limitation, only the outer nuclear layer was examined in this study. The

outer nuclear layer is considered avascular and therefore every hyperreflective foci seen on an OCT scan can be assumed to represent a true candidate focus and not a vessel in cross-section.

In this study, heatmap visualizations often revealed distinct pattern of hyperreflective foci being located in the fovea or close to the optic nerve head. The use of neural networks for the quantification and visualization of hyperreflective foci could assist in tracking subtle intraretinal changes over time that are difficult to detect for even specialists since the magnitude of the change can be very

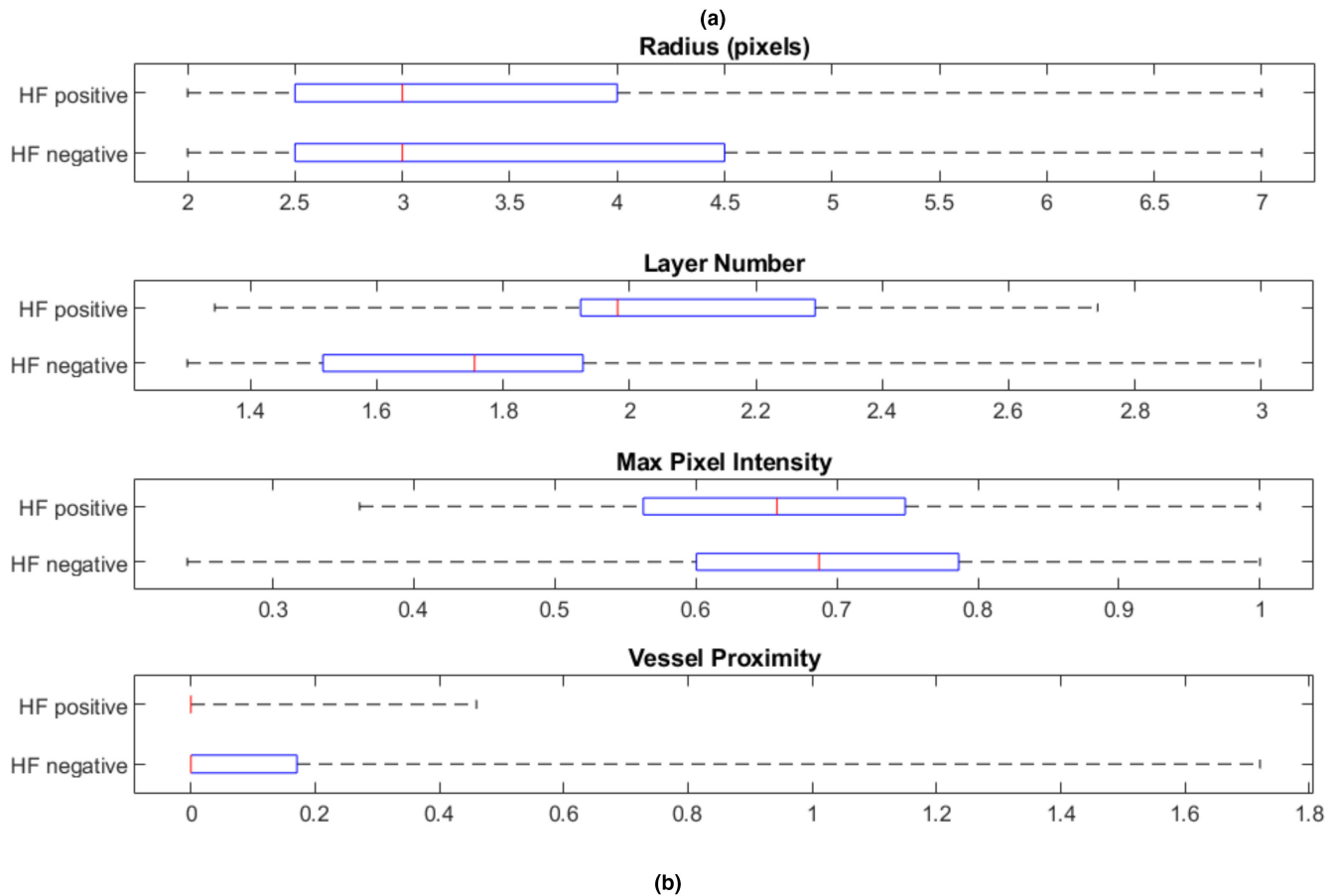


**FIGURE 6** (a) (i) Radius (pixels) shows radius of blobs detected in the pixel unit. One pixel is equal to  $2.5 \mu\text{m}$ . (ii) The layer numbers refer to specific retinal layers and every hyperreflective foci have different anatomical locations corresponding to certain retinal layer numbers. (iii) Max. pixel intensity reflects the brightest pixel contained in blobs detected. (iv) Vessel proximity is a measure of how close a hyperreflective focus is to blood vessels. High values mean close proximity to blood vessels. (b) OCT B-scan with layer numbers marked.

small (Lang et al., 2016). Furthermore, the localization and quantification of the actual size of foci structure in the retina is important. One example is shown in Figure 5 with a central serous chorioretinopathy with detachment of the macula but has the added feature of cystoid oedema. The morphological features are illustrated in great details and the hyperreflective elements that are seen after resolution of the detachment are much larger than the hyperreflective foci we see in healthy subjects.

Limitations of this study include the small sample size and the fact that OCT scans were obtained from only one imaging platform type and not compared with other commercially available OCT devices. However, we would expect to benefit from using a heterogeneous OCT material originating from slightly different OCT scanning protocols on the Heidelberg machines. Regarding

methodological issues all scans need to be examined for motion artefacts arising from averaging. Furthermore, B scans need to be closely spaced in order to thoroughly evaluate hyperreflective foci movement and errors in scan positioning. Due to the distance between B scans a potential variation in the distribution of hyperreflective foci was not considered detectable in this study.

Longitudinal analysis of hyperreflective foci with high-quality OCT data sets may be crucial in future for understanding the pathophysiologic processes underlying disease progression in various retinal disorders. Further prospective studies are necessary to establish the time intervals and transversal resolution needed to sufficiently and accurately detect and track changes in the density and distribution of hyperreflective foci over time in different retinal disorders.

## 5 | CONCLUSIONS

In conclusion, this study demonstrates that automated image analysis and machine learning methods can be applied to successfully identify, quantify and visualize the presence and time-resolved dynamics of hyperreflective foci in the outer nuclear layer of the retina using high-quality OCT scans.

### ORCID

Mathias Falck Schmidt  <https://orcid.org/0000-0001-7086-4638>

### REFERENCES

- Abri Aghdam, K., Pielen, A., Framme, C. & Junker, B. (2015) Correlation between hyperreflective foci and clinical outcomes in neovascular age-related macular degeneration after switching to aflibercept. *Investigative Ophthalmology & Visual Science*, 11, 6448–6455.
- Altay, L., Scholz, P., Schick, T., Felsch, M., Hoyng, C.B., den Hollander, A.I. et al. (2016) Association of hyperreflective foci present in early forms of age-related macular degeneration with known age-related macular degeneration risk polymorphisms. *Investigative Ophthalmology & Visual Science*, 57, 4315–4320.
- Bolz, M., Schmidt-Erfurth, U., Deak, G., Mylonas, G., Kriechbaum, K. & Scholda, C. (2009) Optical coherence tomographic hyperreflective foci: a morphologic sign of lipid extravasation in diabetic macular edema. *Ophthalmology*, 5, 914–920.
- Borrelli, E., Zuccaro, B., Zucchiatti, I., Parravano, M., Querques, L., Costanzo, E. et al. (2019) Optical coherence tomography parameters as predictors of treatment response to eplere-none in central serous chorioretinopathy. *Journal of Clinical Medicine*, 9, 1271.
- Busch, C., Okada, M., Zur, D., Fraser-Bell, S., Rodríguez-Valdés, P.J., Cebeci, Z. et al. (2020) Baseline predictors for visual acuity loss during observation in diabetic macular oedema with good baseline visual acuity. *Acta Ophthalmologica*, 98, 801–806.
- Chen, K.C., Jung, J.J., Curcio, C.A., Balaratnasingam, C., Gallego-Pinazo, R., Dolz-Marco, R. et al. (2016) Intraretinal hyperreflective foci in acquired vitelliform lesions of the macula: clinical and histologic study. *American Journal of Ophthalmology*, 64, 89–98.
- Curcio, C.A., Zanzottera, E.C., Ach, T., Balaratnasingam, C. & Freund, K.B. (2017) Activated retinal pigment epithelium, an optical coherence tomography biomarker for progression in age-related macular degeneration. *Investigative Ophthalmology & Visual Science*, 58, 211–226.
- Fragiotta, S., Abdolrahimzadeh, S., Dolz-Marco, R., Sakurada, Y., Gal-Or, O. & Scuderi, G. (2021) Significance of hyperreflective foci as an optical coherence tomography biomarker in retinal diseases: characterization and clinical implications. *Journal of Ophthalmology*, 21, 567–234.
- Fragiotta, S., Rossi, T., Cutini, A., Grenga, P.L. & Vingolo, E.M. (2018) Predictive factors for development of neovascular age-related macular degeneration. *Retina*, 2, 245–252.
- Framme, C., Wolf, S. & Wolf-Schnurrbusch, U. (2010) Small dense particles in the retina observable by spectral-domain optical coherence tomography in age-related macular degeneration. *Investigative Ophthalmology & Visual Science*, 51, 5965–5969.
- Frizziero, L., Parrozzani, R., Midena, G., Miglionico, G., Vujosevic, S., Pilotto, E. et al. (2016) Hyperreflective intraretinal spots in radiation macular edema on spectral domain optical coherence tomography. *Retina*, 36, 1664–1669.
- Haeker, M., Wu, X., Abramoff, M., Kardon, R. & Sonka, M. (2007) Incorporation of regional information in optimal 3-D graph search with application for intraretinal layer segmentation of optical coherence tomography images. *Information Processing in Medical Imaging*, 4, 12–55.
- Kodjikian, L., Bellocq, D., Banello, F., Loewenstein, A., Chakravarthy, U., Koh, A. et al. (2019) First-line treatment algorithm and guidelines in center-involving diabetic macular edema. *European Journal of Ophthalmology*, 6, 573–584.
- Lang, A., Carass, A., Al-Louzi, O., Bhargava, P., Solomon, S.D., Calabresi, P.A. et al. (2016) Combined registration and motion correction of longitudinal retinal OCT data. *Proceedings of SPIE The International Society for Optical Engineering*, 9784, 97840.
- Lee, H. & Chung, H. (2018) Author response: hyperreflective intraretinal foci as an OCT biomarker of retinal inflammation in diabetic macular edema. *Investigative Ophthalmology & Visual Science*, 13, 53–67.
- Li, K., Wu, X., Chen, D.Z. et al. (2016) Optimal surface segmentation in volumetric images—a graph-theoretic approach. *PAMI*, 2, 78–111.
- Lindeberg, T. (1996) Scale-space: A framework for handling image structures at multiple scales. Proc CERN School of Computing, Edmond aan Zee, The Netherlands 5: 8–21.
- Midena, E., Pilotto, E. & Bini, S. (2018) Hyperreflective intraretinal foci as an OCT biomarker of retinal inflammation in diabetic macular edema. *Investigative Ophthalmology & Visual Science*, 13, 53–66.
- Midena, E., Torresin, T., Velotta, E., Pilotto, E., Parrozzani, R. & Frizziero, L. (2021) OCT hyperreflective retinal foci in diabetic retinopathy: a semi-automatic detection comparative study. *Frontiers in Immunology*, 12, 613–651.
- Mokhtari, M., Ghasemi Kamasi, Z. & Rabbani, H. (2017) Automatic detection of hyperreflective foci in optical Coherence tomography B-scans using morphological component analysis. Proc Annu Int Conf IEEE Eng Med Biol Soc EMBS 8174673461:1497–500.
- Pang, C.E., Messinger, J.D., Zanzottera, E.C., Freund, K.B. & Curcio, C.A. (2015) The onion sign in neovascular age-related macular degeneration represents cholesterol crystals. *Ophthalmology*, 122, 2316–2326.
- Pilotto, E., Mianze, S., Torresin, T., Puthenparampil, M., Frizziero, L., Federle, L. et al. (2020) Hyperreflective foci in the retina of active relapse-onset multiple sclerosis. *Ophthalmology*, 12, 1774–1776.
- Ronneberger, L., Fischer, P. & Brox, T. (2015) U-net: convolutional networks for biomedical image segmentation. Published in *MICCAI Computer Science*, 7, 234–345.
- Torm, W., Belmouhand, M., Munch, I.C. et al. (2020) Migration of an outer retinal element in a healthy child followed by longitudinal multimodal imaging. *American Journal of Ophthalmology Case Reports*, 18, 100637.
- Uji, A., Murakami, T., Nishijima, K., Akagi, T., Horii, T., Arakawa, N. et al. (2012) Association between hyperreflective foci in the outer retina, status of photoreceptor layer, and visual acuity in diabetic macular edema. *American Journal of Ophthalmology*, 153, 710–717.
- Varga, L., Kovács, A., Grósz, T., Thury, G., Hadarits, F., Dégi, R. et al. (2019) Automatic segmentation of hyperreflective foci in OCT images. *Computer Methods and Programs in Biomedicine*, 178, 91–103.
- Vujosevic, S., Bini, S., Midena, G., Berton, M., Pilotto, E. & Midena G. (2013) Hyperreflective intraretinal spots in diabetics without and with nonproliferative diabetic retinopathy: an in vivo study using spectral domain OCT. *J Diabetes Res*, 13, 489–838.
- Wang, M., Ma, W., Zhao, L., Fariss, R.N. & Wong, W.T. (2011) Adaptive Müller cell responses to microglial activation mediate neuroprotection and coordinate inflammation in the retina. *Journal of Neuroinflammation*, 8, 173–191.
- Yu, C., Xie, S., Niu, S., Ji, Z., Fan, W., Yuan, S. et al. (2019) Hyperreflective foci segmentation in SD-OCT retinal images with diabetic retinopathy using deep convolutional neural networks. *Medical Physics*, 46, 4502–4519.

**How to cite this article:** Schmidt, M.F., Christensen, J.L., Dahl, V.A., Toosy, A., Petzold, A. & Hanson, J.V.M. et al. (2022) Automated detection of hyperreflective foci in the outer nuclear layer of the retina. *Acta Ophthalmologica*, 00, 1–7. Available from: <https://doi.org/10.1111/aos.15237>